Supporting Information

An Atomically Defined Iron Carbide Surface for Fischer-Tropsch Synthesis Catalysis

Yijia Li,[†] Zheshen Li,[‡] Ali Ahsen,[§] Lutz Lammich,[†] Gilbére J. A. Mannie,[‖] J.W. (Hans) Niemantsverdriet,[‖,⊥] Jeppe V. Lauritsen [†,]*

[†]Interdisciplinary Nanoscience Center, Aarhus University, DK-8000 Aarhus C, Denmark.

[‡]Institute for Storage Ring Facilities, Aarhus University, 8000 Aarhus, Denmark.

[§]Department of Physics, Science Faculty, Gebze Institute of Technology, 41400 Gebze, Kocaeli, Turkey.

[‖]SynCat@Beijing, Synfuels China Technology Co. Ltd., Huairou, Beijing 101407, China.

[⊥]SynCat@DIFFER, Syngaschem BV, PO Box 6336, 5600 HH, Eindhoven, The Netherlands.

* E-mail: jvang@inano.au.dk

S1. Estimation of sensitivity factor

It is possible to analyze the XPS spectra and determine the Fe:C ratio by using peak area and peak height sensitivity factors. However, the peak sensitivity factors vary depending on many parameters such as light source, photon energy, and electron analyzer. Therefore, we have used a calibration sample to check the sensitivity factors for carbon and iron signals at Matline, ASTRID2 synchrotron.
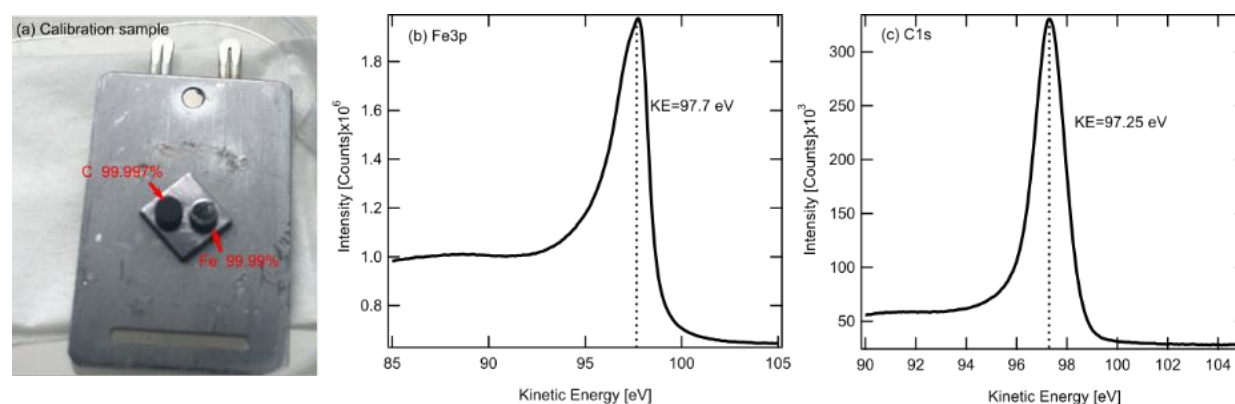

Figure S1 (a) Image of the calibration sample. The two small cylinders are cut from rod materials of Fe and C used for e-beam evaporators. (b,c) XPS spectra used for sensitivity factor calibration. The Fe3p spectrum was acquired with a PE of 150 eV, the C1s spectrum at 380 eV.

The calibration sample is made of two small cylinders cut from rod materials of Fe (99.99%, Goodfellow) and C (99.997%, Goodfellow) used for e-beam evaporators. The as-cut cross sections were made as flat as possible and the heights and surface areas of the two cylinders were kept the same. They were fixed on a piece of plate, which was soldered onto the sample holder (Figure S1a). Cycles of sputtering and annealing were used to remove impurities and oxide layer on the surfaces. The purity was checked by XPS. The data acquisition parameters such as energy window and step size were kept the same as for the actual XPS experiments, and so were the photon energies (150 and 380 eV for Fe and C, respectively).

The kinetic energies of the photoelectrons were almost the same for both peaks, as shown in Figure S1b and c, indicating that the inelastic mean free paths of the electrons are comparable.

The ratio of the sensitivity factors for Fe and C can be derived from the measured peak areas as:

$$\frac{S_{Fe}}{S_C} = \frac{A_{Fe}}{A_C} = 7.5 \pm 0.5 \,,$$

where A is the peak area and S is the sensitivity factor. (Note the different scales in Figure S1b and c.) Before integrating the peak areas, linear backgrounds were subtracted in both regions. Therefore, the Fe:C ratio in the iron carbide sample can be calculated as:

$$\frac{n_C}{n_{Fe}} = \frac{\dfrac{A_{C,carbide}}{S_C}}{\dfrac{A_{Fe,carbide}}{S_{Fe}}} = \frac{A_{C,carbide}}{A_{Fe,carbide}} \frac{S_{Fe}}{S_C}$$

where A is the integrated peak area for carbide carbon or iron. For the Fe3p peak area integration, a linear background and the Au5f peak are subtracted from the Fe3p signal. For the carbide peak area estimation, only the carbidic carbon component is used.

For estimating the C deposition rate, the C coverage is back-calculated by using the sensitivity factor ratio and the known Fe coverage. Since the total amount of C should be calculated, the sum of carbidic, sp^2 and sp^3 carbon peak areas are sued for A_C.

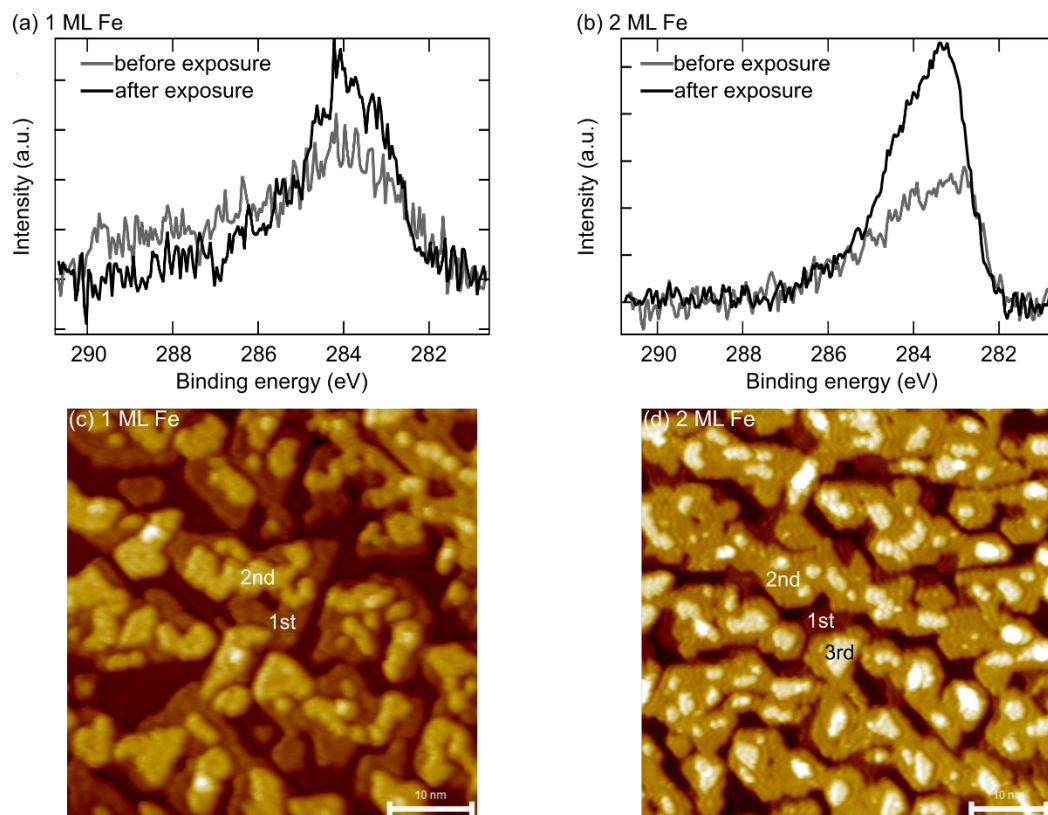## S2. The influence of the Fe films thickness on ethylene decomposition

Figure S2. (a-b) XPS spectra show the C1s signal change after C_2H_4 exposure to 1 ML and 2 ML Fe films supported on Au(111). The gray spectra reflect the state before C_2H_4 exposure, while the black spectra correspond to the state after exposure. After the same dosage of C_2H_4, only the C1s spectrum for the 2 ML Fe/Au(111) film exhibits a significant increase in the intensity, indicating C_2H_4 decomposition occurs on this surface. (c-d) STM images of Fe films on Au(111) with coverage of 1 ML and 2 ML, respectively. The appearance of the third-layer structure is the onset of the phase transformation from *fcc*(111) to *bcc*(110) according to the literature.[1, 2]

In order to explore the C_2H_4 decomposition on Fe/Au(111) films, XPS measurements were performed to monitor the C species change in the sample after C_2H_4 exposure. Figure S2a and b show XPS spectra of

the C1s region acquired before (gray) and after (black) C_2H_4 exposure (3×10^{-6} mbar, RT, 10 min) of 1 ML (S2a) and 2 ML (S2b) Fe/Au(111) films. The small carbon signal from the metallic Fe films before C_2H_4 exposure is due to carbon-containing contaminations under UHV conditions. As shown in Figure S2a, C_2H_4 exposure of 1 ML Fe/Au(111) films causes no significant changes in the C1s signal. In contrast, in case of 2 ML Fe/Au(111), the carbon intensity is increased significantly after exposure, indicating that C_2H_4 decomposition occurs on this surface.

STM measurements were performed in order to correlate the Fe film topography with the C_2H_4 decomposition reactivity. As illustrated in Figure S2c and d, the structure changes with increasing thickness of the Fe films. For 1 ML Fe film (Figure S2c), there are mainly two atomic layers of Fe involved in the growth, which increases to three at the coverage of 2 ML (Figure S2d). The third layer structure indicates a phase transformation from *fcc*(111) to *bcc*(110) occurring on Fe/Au(111) films.[1, 2] We therefore correlate the C_2H_4 decomposition with the emergence of *bcc* structure in the Fe films.

Table S1. Literature reports of C1s binding energies for sp^3, sp^2 and carbidic carbon in iron carbide samples.

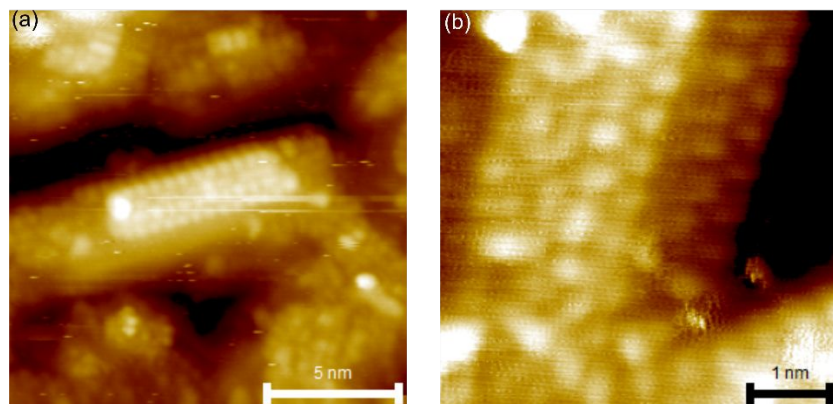| Reference	sp^3 (eV)	sp^2 (eV)	Carbide (eV)
3, 4	285	284.3-284.9	283.3
5	-	-	282.1
6	285.4	284.2	283.4
7	-	-	283.5
8	285.4	284.65	285.37
9, 10	-	284.9	283.4
11	-	284.6	283.5
12	-	284.5	283.2
13, 14	285.1	284.2	283.4
15	-	-	282.7

Figure S3. (a) Large-scale STM image showing the same region with Figure 6b. (b) Additional atom-resolved STM image shows the top facet of one carbide patch, exhibiting the perturbed (2×2) reconstructed structure.
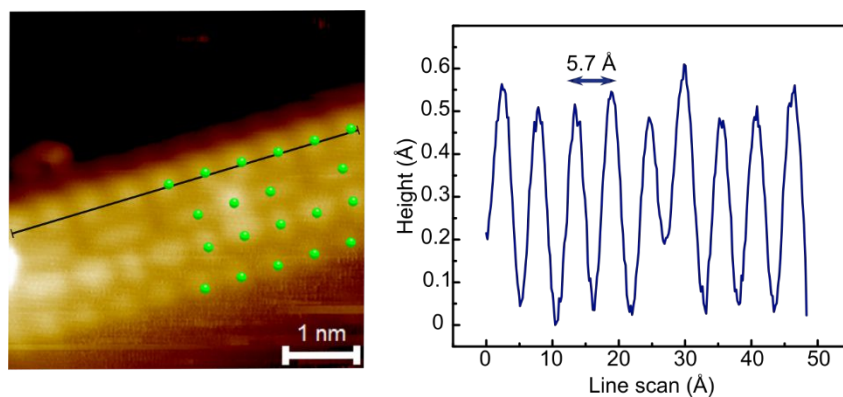

Figure S4. Line profile of the STM image in Figure 6b. The distance between two protrusions along the long edge is ~5.7 Å.

References

(1) Bulou, H.; Scheurer, F.; Ohresser, P.; Barbier, A.; Stanescu, S.; Quirós, C., Structure of Self-Organized Fe Clusters Grown on Au(111) Analyzed by Grazing Incidence X-Ray Diffraction. *Phys. Rev. B* **2004,** *69*, 155413.
(2) Allmers, T.; Donath, M., Growth and Morphology of Thin Fe Films on Flat and Vicinal Au(111): A Comparative Study. *New J. Phys.* **2009,** *11*, 103049.

(3) Furlan, A.; Lu, J.; Hultman, L.; Jansson, U.; Magnuson, M., Crystallization Characteristics and Chemical Bonding Properties of Nickel Carbide Thin Film Nanocomposites. *J. Phys.: Condens. Matter* **2014,** *26*, 415501.

(4) Furlan, A.; Jansson, U.; Lu, J.; Hultman, L.; Magnuson, M., Structure and Bonding in Amorphous Iron Carbide Thin Films. *J. Phys.: Condens. Matter* **2015,** *27*, 045002.

(5) Booyens, S.; Gilbert, L.; Willock, D.; Bowker, M., The Adsorption of Ethene on Fe(111) and Surface Carbide Formation. *Catal. Today* **2015,** *244*, 122-129.

(6) Yang, C.; Zhao, H.; Hou, Y.; Ma, D., Fe5c2 Nanoparticles: A Facile Bromide-Induced Synthesis and as an Active Phase for Fischer-Tropsch Synthesis. *J. Am. Chem. Soc.* **2012,** *134*, 15814-15821.

(7) Arabczyk, W.; Storbeck, F.; Müssig, H. J., Electron Spectroscopy Studies on Carbon Segregation from a Mono-Crystalline A-Fe(111) Specimen. *Appl. Surf. Sci.* **1993,** *65*, 94-98.

(8) Liang, Y.; Liu, P.; Xiao, J.; Li, H.; Wang, C.; Yang, G., A Microfibre Assembly of an Iron-Carbon Composite with Giant Magnetisation. *Sci Rep.* **2013,** *3*, 3051.

(9) Vinogradov, N. A.; Zakharov, A. A.; Kocevski, V.; Rusz, J.; Simonov, K. A.; Eriksson, O.; Mikkelsen, A.; Lundgren, E.; Vinogradov, A. S.; Martensson, N.; Preobrajenski, A. B., Formation and Structure of Graphene Waves on Fe(110). *Phys. Rev. Lett.* **2012,** *109*, 026101.

(10) Vinogradov, N. A.; Simonov, K. A.; Generalov, A. V.; Drnec, J.; Carlà, F.; Vinogradov, A. S.; Preobrajenski, A. B.; Mårtensson, N.; Felici, R., The Structural Evolution of Graphene/Fe(110) Systems Upon Annealing. *Carbon* **2017,** *111*, 113-120.

(11) Panzner, G.; Diekmann, W., The Bonding State of Carbon Segregated to A-Iron Surfaces and on Iron Carbide Surfaces Studied by Electron Spectroscopy. *Surf. Sci.* **1985,** *160*, 253-270.

(12) Park, E.; Zhang, J. Q.; Thomson, S.; Ostrovski, O.; Howe, R., Characterization of Phases Formed in the Iron Carbide Process by X-Ray Diffraction, Mossbauer, X-Ray Photoelectron Spectroscopy, and Raman Spectroscopy Analyses. *Metall. Mater. Trans. B* **2001,** *32*, 839-845.

(13) Wiltner, A.; Linsmeier, C., Formation of Endothermic Carbides on Iron and Nickel. *Phys. Status Solidi A* **2004,** *201*, 881-887.

(14) Wiltner, A.; Linsmeier, C.; Jacob, T., Carbon Reaction and Diffusion on Ni(111), Ni(100), and Fe(110): Kinetic Parameters from X-Ray Photoelectron Spectroscopy and Density Functional Theory Analysis. *J. Chem. Phys.* **2008,** *129*, 084704.

(15) Zhou, X.; Mannie, G. J. A.; Yin, J. Q.; Yu, X.; Weststrate, C. J.; Wen, X. D.; Wu, K.; Yang, Y.; Li, Y. W.; Niemantsverdriet, J. W., Iron Carbidization on Thin-Film Silica and Silicon: A near-Ambient-Pressure X-Ray Photoelectron Spectroscopy and Scanning Tunneling Microscopy Study. *ACS Catal.* **2018,** *8*, 7326-7333.